Experimental trajectories of two drops in planar extensional flow

Derek C. Tretheway, Masahiro Muraoka,[a] and L. Gary Leal[b]
Department of Chemical Engineering, University of California, Santa Barbara, Santa Barbara, California 93106

(Received 23 September 1998; accepted 29 January 1999)

In this paper we map the experimental trajectories of two deformable drops in planar extensional flow and compare the experimental results with theoretical calculations for spherical drops. We examine the effects that deformation, initial position, and viscosity ratio have on the interaction of two drops and the necessity of incorporating deformation into trajectory calculations, which can be used to estimate the collision rates, the collision efficiencies, and the collision interaction times. For drops which do not come into close contact, the existing theoretical calculations for spherical drops accurately predict the symmetric trajectories and capture the increased hydrodynamic interaction for higher viscosity ratios. For drops which come into close contact, the spherical drop theory accurately predicts the approach and exit trajectories and with a slight empirical modification adequately predicts the interaction times for deformable drops with a Taylor deformation parameter up to 0.22. The experimental results show that for drops with close contact, the collision trajectories are asymmetric and irreversible with a minimum separation between the centers of mass that is less than the minimum separation of two spheres. This minimum separation corresponds to the minor axis of the deformed drop and is not captured by the spherical theory. However, overall, the modified trajectory theory based upon the hydrodynamic mobility for spherical drops does provide a reasonable estimate for the trajectories and the interaction times for two deformable drops in planar extensional flow. © *1999 American Institute of Physics.* [S1070-6631(99)02905-0]

I. INTRODUCTION

The coalescence and breakup of drops immersed in an immiscible suspending fluid plays an integral role in many industrial, biological, and natural processes such as liquid–liquid extraction and polymer blending. In the limit of dilute systems, breakup involves only a single drop in a suspending fluid, but coalescence requires two drops to collide and remain together for a sufficient amount of time for film drainage to occur. Thus, the coalescence probability, which incorporates the collision rate and the interaction time, depends directly on the hydrodynamic interaction between two drops. As a result, coalescence studies are more difficult from both an experimental and theoretical perspective, and relatively less has been done than for the case of drop breakup. It is traditional in studies of coalescence to assume that the problem can be split into two parts; the collision process and a film drainage process. A great deal of work has been done on the film drainage problem. In reality, however, many of the details of film drainage depend upon the initial shape of the film, and on the forces which are acting on the two drops while they are in close proximity to one another. Thus, at least from a quantitative point of view, it is impossible to avoid considering the complete drop collision and interaction process, and it is this overall process which has not yet received extensive investigation. Indeed, a complete theoretical framework is only available for two spherical drops.

The creeping flow problem of two spherical particles interacting in a linear flow field was, in fact, first solved by Batchelor and Green,[1] who examined the hydrodynamic interactions between two rigid spheres with the objective of determining the particle contribution to the mean stress in a nondilute suspension of spherical particles. Much more recently, Wang, Zinchenko, and Davis[2] extended Batchelor and Green's[1] analysis to investigate the hydrodynamic interaction between two spherical drops immersed in a linear flow field. By calculating the trajectories, the effects of hydrodynamic interactions on the collision efficiencies and thus coalescence probability were examined for two spherical drops. While these theoretical results for spheres provide insight into the collision process, drops in actual systems are never precisely spherical. As a result, more recent theoretical and computational work has concentrated on using the boundary integral technique to study numerically the interaction of deformable drops in the creeping flow limit. Lowenberg and Hinch[3] studied the collision of two deformable drops in a shear flow. Zinchenko, Rother, and Davis[4] studied the buoyancy-driven interaction of two deformable drops. Manga and Stone[5] examined the buoyancy-driven interaction of two, three, and four deformable drops. While theoretical work continues to advance, experimental studies with which to confirm the theoretical calculations are quite limited. Zhang, Davis, and Ruth[6] have examined experimentally the buoyancy-driven interaction between two nearly spherical drops, with results that agree with theoretical calculations for spheres, while Manga and Stone[5,7] have examined the buoyancy-driven interaction between two highly deformable

[a]Department of Mechanical Engineering, Science University of Tokyo, Noda, Japan.
[b]Author to whom all correspondence should be addressed.

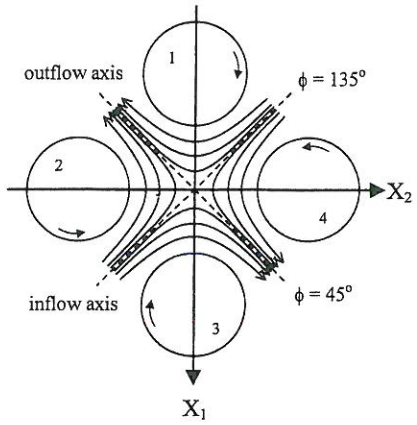

FIG. 1. Schematic of the four roll mill (top view) with the experimental flow field in the drop trajectory coordinate system (see Fig. 2).

drops. Guido and Simeone[8] studied the binary collision of two drops in shear flow. Their results showed good agreement with the numerical simulations of Lowenberg and Hinch,[3] but a direct comparison with the trajectory predictions for spherical drops was not included.

Since it is cumbersome, at best, to combine boundary integral calculations with trajectory calculations for simulations of large-scale systems with many drops, a key issue in developing a theoretical basis for design in mixing and dispersion applications is to determine conditions where the theoretical calculations for spherical drops can provide a sufficiently accurate representation of the collision process. Since the collision and interaction process depends strongly on the undisturbed flow, the full range of flow types needs to be examined to test fully the theory for spherical drops. In this work, we complement previous works on shear flow and the buoyancy-driven motion of drops by examining two drops in a qualitatively different flow, two-dimensional (2-D) extensional flow. We map the experimental trajectories of two deformable drops in 2-D extensional flow and compare the experimental results with theoretical calculations for spherical drops. We examine the effect deformation has on the interaction of two drops and the necessity of incorporating deformation into the theoretical calculations that are used to estimate the collision rates, the collision efficiency, and the interaction times of two drops.

II. EXPERIMENTAL SYSTEM

A. Experimental apparatus

The trajectories of two drops are mapped in the four roll mill, an experimental apparatus which has been used extensively in the study of drop deformation and breakup. Figure 1 provides a schematic of the four roll mill. It consists of four vertical cylinders immersed in a fluid bath. The rollers are rotated to produce a flow field in which the velocity gradient is approximately independent of position at the center of the device. By varying the individual roller rotation rates, flows with an arbitrary ratio of strain rate to vorticity can be generated. In Cartesian coordinates the velocity gradient tensor near the center of the four roll mill is given by

TABLE I. Physical properties of experimental fluids.

Fluid	Density (g/cm^3)	Viscosity (poise)	Interfacial tension (dyne/cm)
Suspending fluid			
Pale 170/Pale 1000 blend	1.0	160.7	
Drop fluids			
Dow Corning 200, 60,000 cS fluid	0.97	594.4	5.43
Dow Corning 510, 500 cS fluid	0.97	4.82	5.09

$$\nabla \mathbf{u} = \frac{\gamma}{2}\begin{bmatrix} 1+\alpha & 1-\alpha & 0 \\ -1+\alpha & -1-\alpha & 0 \\ 0 & 0 & 0 \end{bmatrix}, \tag{1}$$

where α is the flow type parameter and γ is the "shear" rate. The parameter α provides a measure of the relative magnitude of the strain rate to vorticity,

$$\frac{\text{magnitude of strain rate}}{\text{magnitude of vorticity}} = \frac{1+\alpha}{1-\alpha}.$$

Thus, $\alpha = 1$ for pure extensional flow, $\alpha = -1$ for pure rotational flow, and $\alpha = 0$ for shear flow.

Details of the four roll mill and its corresponding control algorithm are given in Bentley and Leal[9] with additional modifications outlined in Milliken and Leal.[10] The four roll mill consists of a 49.5 cm square by 17.5 cm deep box filled with the suspending fluid. Four rollers, 15.5 cm long with a radius of 5.0 cm, are centered at the corners of a 12.54 cm by 12.54 cm square. This provides a roller gap width of 2.54 cm and a ratio of roller spacing to roller radius of 1.25. The four rollers are driven by four independent dc stepping motors which are geared down by planetary and worm gears to produce a shear rate between 0.005 and 0.5 s^{-1}. The rollers are immersed in the suspending fluid, a highly viscous Newtonian oil, which is floated on a thin layer of mercury at the bottom of the apparatus. The mercury provides an approximate stress free surface (slip surface) which reduces edge effects from the bottom of the apparatus and limits secondary flows. A small Plexiglas™ window extends through the mercury layer, which enables the drop to be visualized from the bottom. The drops are illuminated from above by a collimated beam of light.

B. Experimental fluids

Table I provides the relevant physical properties of the suspending and drop fluids. The four roll mill is filled with a modified castor oil (a blend of CasChem Pale 1000 and Pale 170 oils). On a Rheometrics model DSR rheometer, this blend displays a shear viscosity that is independent of shear rate and does not exhibit significant normal stresses up to a shear rate of 10 s^{-1}. For the current experimental studies, the shear rate never exceeds 0.05 s^{-1}. Thus at the shear rates of interest, the suspending fluid behaves as a viscous Newtonian fluid. We suspend in the modified castor oil, silicon-based neutrally buoyant, immiscible, Newtonian drops (Dow Corning 200 and 510 fluids) which have radii of approximately 1.0–1.5 mm. The selection of these fluids allows us to examine viscosity ratios that vary between 0.03 and 3.70

with interfacial tensions of approximately 5.0 dyn/cm. The interfacial tensions are determined by comparing the drop deformation in a weak extensional flow ($\alpha=1$) to small deformation theory. As shown in previous drop deformation experiments (Bentley and Leal,[9] Milliken and Leal[10]), small deformation theory provides an accurate measure of the interfacial tension.

C. Experimental procedure

By following the procedure outlined below, we are able to produce and examine the interaction of two equal size drops in the plane of flow. First, a single drop is injected into the four roll mill and subjected to an extensional flow while the four roll mill control scheme maintains the drop at the center of the device. The shear rate is raised above the critical shear rate and held until the drop extends past its critical deformation for breakup. The flow is then stopped and the drop breaks by the capillary pinching mechanism described in previous experimental studies (Bentley and Leal,[9] Stone and Leal[11]). While it is ideal for the initial drop to break into only two drops, if the drop is extended too far, it will break into more than two drops when the flow is stopped. If this occurs, the most common outcome was three drops in this work (two equal size drops and one small satellite drop), the satellite drop was removed without disturbing the primary drops (shifting the drops out of plane). This is accomplished by centering the satellite drop at the stagnation point of the four roll mill, and applying an extensional flow with the active control scheme until the primary drops move sufficiently outside the central region of the four-roll mill. The isolated satellite drop (or drops) is then removed with a small syringe, and the primary drops are brought back into the central region by reversing the flow. The above procedure thus yields two equal size drops in the same horizontal plane. The two drops are then adjusted to the desired initial relative position (with independent computer control of the four rollers, we can basically pick any desired initial position), and the motors are then engaged without the control scheme to produce the desired flow field. The trajectories are mapped by taking photos with a 35 mm camera at known times. The negatives are then analyzed to obtain the positions of the drops.

III. THEORETICAL TRAJECTORIES

For two spherical Newtonian drops suspended in a second immiscible Newtonian fluid and subjected to an ambient linear flow field under creeping flow conditions, the relative velocity of the two drops can be expressed as (neglecting nonhydrodynamic interdroplet forces)

$$\mathbf{V}_{12}=\boldsymbol{\Omega}\cdot\mathbf{r}+\mathbf{E}\cdot\mathbf{r}-\left[A(s)\frac{\mathbf{rr}}{r^2}+B(s)\left(\mathbf{I}-\frac{\mathbf{rr}}{r^2}\right)\right]\cdot\mathbf{E}\cdot\mathbf{r}, \quad (2)$$

where r is the vector from the center of drop 1 to the center of drop 2, $s=2r/(a_1+a_2)$ is the dimensionless center to center distance (a_1 and a_2 are the radii of the two drops, respectively), $\boldsymbol{\Omega}$ is the vorticity tensor, $\mathbf{E}$ is the rate of strain tensor, $A(s)$ is the relative mobility function along the drops' line of center, and $B(s)$ is the relative mobility function perpendicular to the drops' line of center. $A(s)$ and $B(s)$ depend on the dimensionless separation (s), the viscosity ratio ($=\mu_{\text{drop}}/\mu_{\text{susp}}$), and the size ratio of the two drops. Details and derivations of $A(s)$ and $B(s)$, based on a bispherical coordinate system, are provided in Wang, Zinchenko, and Davis.[2] Values of $A(s)$ and $B(s)$ calculated with the Wang *et al.*[2] formulas are accurate for dimensionless gaps (s-2) greater than 10^{-6}. Below this dimensionless gap, $A(s)$ and $B(s)$ cannot be calculated accurately due to the singularity in the coordinate expressions for $A(s)$ and $B(s)$.

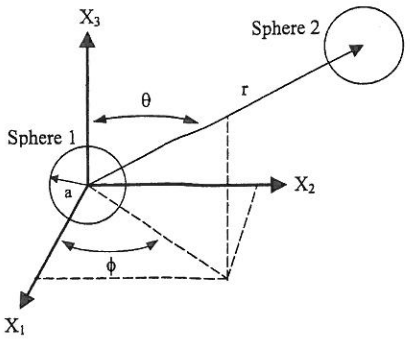

FIG. 2. Coordinate system for trajectory calculations.

The relative velocity of the two drops can be decomposed into motions along and normal to their line of centers to provide the trajectory equations for the two drops. The trajectories are described in a coordinate system, shown in Fig. 2, which is consistent with previous theoretical work. Here, θ is the out-of-plane orientation angle, ϕ is the in-plane orientation angle, and r was defined previously. In addition to providing a top view of the four-roll mill, Fig. 1 shows the experimental flow field in the defined coordinate system. When $\phi=135°$ the line of centers of the two drops is aligned parallel to the inflow axis of the undisturbed flow, when $\phi=45°$ the drops are aligned parallel to the outflow axis, and when $\phi=90°$ the pair of drops is just rotating from the compressional (inflow) quadrant to the extensional (outflow) quadrant of the flow.

Substituting the vorticity and rate of strain tensors for a general two-dimensional linear flow, Eq. (1), into the relative velocity equation, Eq. (2), yields the dimensionless trajectory equations

$$\frac{ds}{dt}=\gamma s(1+\alpha)(1-A(s))\sin^2\theta\sin\varphi\cos\varphi, \quad (3)$$

$$\frac{d\theta}{dt}=\gamma(1+\alpha)(1-B(s))\sin\varphi\cos\varphi\cos\theta\sin\theta, \quad (4)$$

$$\frac{d\varphi}{dt}=\gamma\left[\cos^2\varphi\left(\alpha-\frac{B(s)}{2}(1+\alpha)\right)-\sin^2\varphi\left(1-\frac{B(s)}{2}(1+\alpha)\right)\right]. \quad (5)$$

For the experimental conditions of pure extensional flow ($\alpha=1$) and in-plane interaction of the two drops (θ

$=\pi/2$), Eqs. (3)–(5) reduce to two equations, an equation for the dimensionless separation, s, and an equation for the in-plane orientation angle, ϕ,

$$\frac{ds}{dt^*}=2s(1-A(s))\sin\varphi\cos\varphi, \tag{6}$$

$$\frac{d\varphi}{dt^*}=(1-B(s))[2\cos^2\varphi-1], \tag{7}$$

where time t^* is nondimensionalized with the shear rate. Equations (6) and (7) are solved with a Runga–Kutta–Verner fifth-order and sixth-order method, with the initial drop positions chosen to match those of the experimental study. As expected, solutions of Eqs. (6) and (7) indicate that purely spherical drops collide (coalescence) if the drops are sufficiently aligned relative to the inflow axis. In the experimental study, however, it is found that the thin film drainage time exceeds the interaction time and coalescence is not observed for the range of capillary numbers and drop sizes studied due to the additional interfacial deformation that develops between two drops in close contact. We will discuss this further in a later section. To estimate both the approach and exit trajectories, as well as the "interaction time" when the drops are in a close contact configuration, without actually incorporating deformation, we resort to an *ad hoc* procedure which forces the spherical drops to remain separated, yet allows the drops to rotate with the rotation rate predicted from Eq. (7) with $s=2$. This modification is applied to the solutions of Eq. (6) just before the spherical drops collide and is equivalent to introducing a nonhydrodynamic repulsive force that keeps the spherical drops from coalescing. This modification is implemented numerically when the drops are in the compressional quadrant of the flow ($\phi>90°$) and the computed dimensionless gap (s-2) is less than 10^{-6}. The modification sets the equation for the dimensionless separation [Eq. (6)] to zero and fixes $s=2.000\,001$ in Eq. (7). Thus, the in-plane orientation angle (ϕ) continues to evolve with a constant $B(s)$ [$B(s)$ approaches a constant value for gaps less than 10^{-4}]. The continued evolution of ϕ preserves the rotation rate and allows for an estimation of the interaction time. When the pair of drops rotates from the compressional quadrant ($\phi>90°$) to the extensional quadrant ($\phi<90°$), the *ad hoc* modification is relaxed and the complete spherical theory, Eqs. (6) and Eq. (7), resumes. The above *ad hoc* modification has been previously implemented by Lowenberg and Hinch[3] to stabilize spherical drops against coalescence in their numerical study on the collision of two deformable drops in shear flow.

IV. RESULTS

A. Rigid solid spheres

The trajectories of two solid rigid spheres are mapped in the experimental apparatus and compared to theoretical predictions for spherical drops with an infinite viscosity ratio to verify the experimental methods. Values of the mobility functions, $A(s)$ and $B(s)$, approach the rigid, solid limit at a viscosity ratio of 100. Above this viscosity ratio, the values of $A(s)$ and $B(s)$ are essentially constant for increasing viscosity ratios. A viscosity ratio of 10^6 was chosen for the theoretical calculations. Figure 3 shows the shape of the relative trajectories (s vs ϕ), whereas Figs. 4 and 5 show the time dependence of s and ϕ, respectively, for two rigid spheres. It should be noted that the bold line in these figures (and in all that follow) represents the trajectories that would be followed if the contours of the drops followed streamlines of the base flow [Eq. (1)], whereas the lighter line is the trajectory calculated for spherical drops using the theory described in the preceding section. We show both a case where the spheres remain sufficiently separated for all time (i.e., $s>2$), and a case where the spheres nearly touch. Excellent agreement between the theoretical predictions and the experimental results is obtained. When compared to hypothetical spheres that move affinely along the streamlines of the undisturbed flow, the effect of the hydrodynamic interaction between the two spheres is to shift the minimum separation to larger values and retard both the approach rate and rotation speed of the two spheres. Of course, the relative trajectory curves for smooth spheres should be symmetric whether hydrodynamic interactions are present or not. On the other hand, if the surface roughness of the spheres were compa-

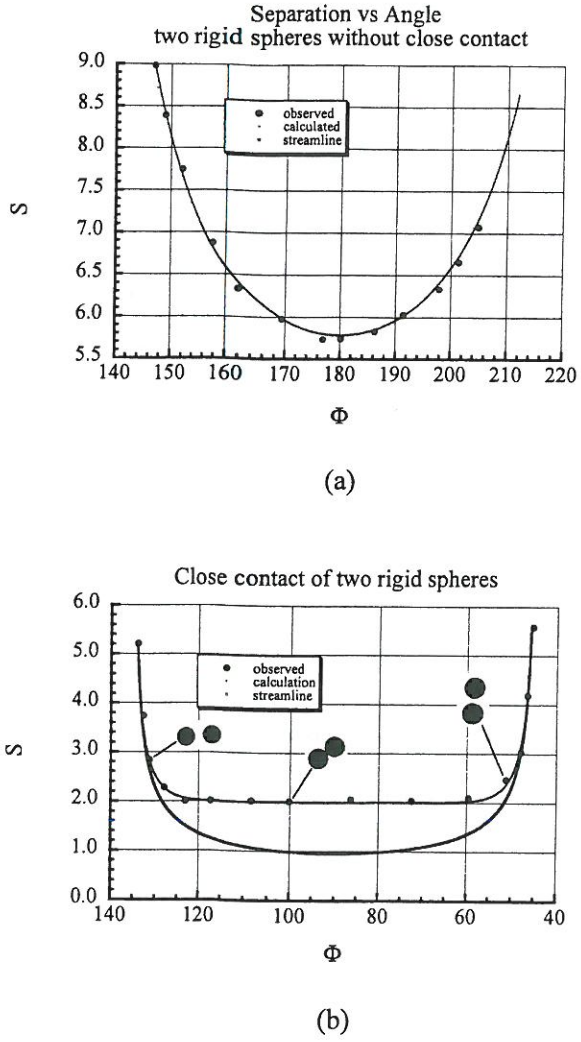

FIG. 3. Relative trajectories, S vs ϕ, for rigid spheres (a) without close contact, (b) with close contact.

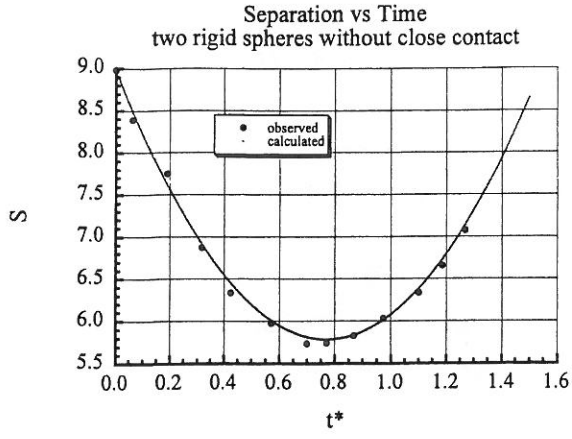

(a)

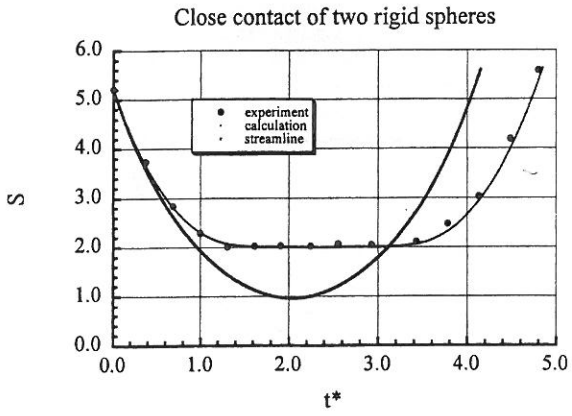

(b)

FIG. 4. Time dependence of S for rigid spheres (a) without close contact, (b) with close contact.

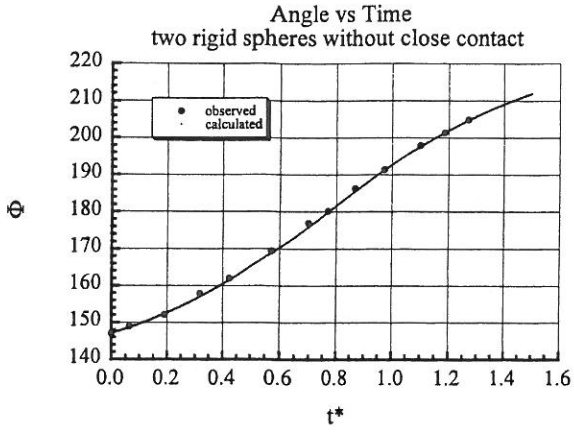

(a)

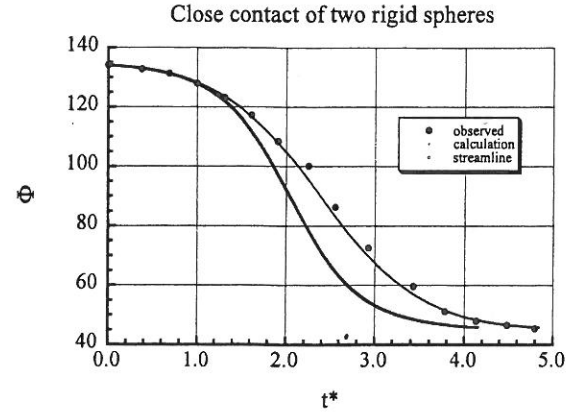

(b)

FIG. 5. Time dependence of ϕ for rigid spheres (a) without close contact, (b) with close contact.

rable to the dimensionless gap, an asymmetry in the relative trajectory curves should develop for spheres in close contact. Since, within error, no asymmetry is observed experimentally, the surface roughness must be smaller than the dimensionless gaps observed and insignificant to the interaction. We can confirm this by comparing the measured minimum gap to the surface roughness of the spheres. From the measured minimum separation of the sphere centers, the minimum gap separating the two surfaces is 13 μm. This distance is slightly larger than the surface roughness (no larger than 5 μm) estimated from scanning electron microscopy imaging of the particle surfaces and agrees with our observations of a symmetric trajectory curve.

B. Noncolliding drops

The capillary number ($\mathrm{Ca}=a\mu\gamma/\sigma$, where a is the undeformed drop radius, μ is the viscosity ratio of the suspending fluid, γ is the shear rate, and σ is the interfacial tension) provides a measure of the ratio of viscous forces to interfacial forces acting on a drop. As the capillary number increases, the viscous forces increase relative to the interfacial forces and the drop deforms. A measure of the deformation for small deformations is the Taylor deformation parameter, $D_f=(L-B)/(L+B)$, where L is the length of the drop and B is the breadth of the drop.

First, we examine the effects of the viscosity ratio and the initial orientation angle, ϕ, on the trajectories of two drops, whose initial position is such that they remain separated by a distance comparable to their radius. As the viscosity ratio increases, the hydrodynamic interaction between the two drops should increase according to (6) and (7). Thus, relative to lower viscosity ratio drops, higher viscosity ratio drops should deviate from undisturbed streamlines at larger separations and for initial orientations that are less aligned with the inflow axis. Figure 6 shows the "shapes" of the relative trajectories, whereas Figs. 7 and 8 provide the time dependence of s and ϕ for two viscosity ratios, 0.03 ($\mathrm{Ca}=0.01$, $D_f=0.034$) and 3.70 ($\mathrm{Ca}=0.015$, $D_f=0.043$), with initial orientations that are not aligned with the inflow axis. For a viscosity ratio of 0.03, the initial orientation is sufficiently offset from the inflow axis that the drop interaction is insignificant and the trajectories are identical to the trajectories of material points following the undisturbed streamlines. The theoretical calculation for spherical drops also predicts

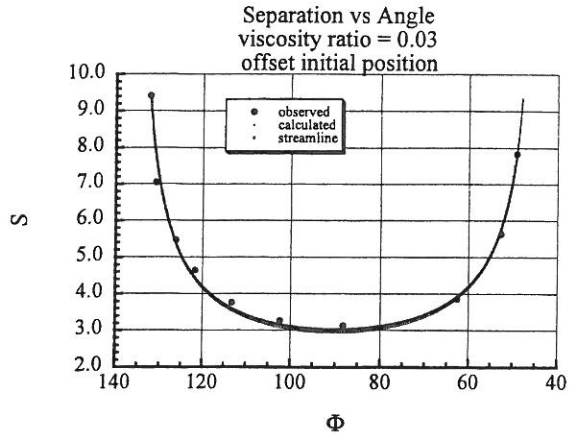

(a)

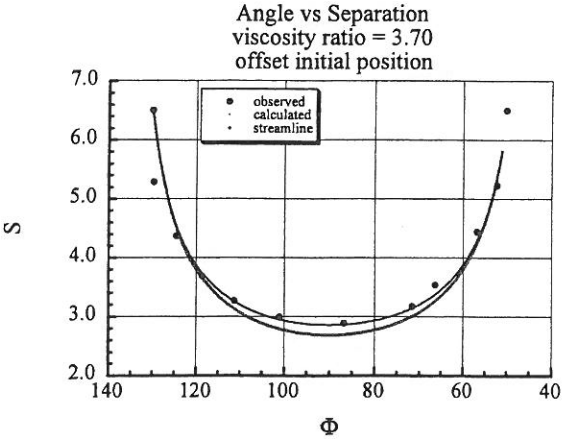

(b)

FIG. 6. Relative trajectories, S vs ϕ, for drops offset from the inflow axis (a) $\lambda = 0.03$, (b) $\lambda = 3.70$.

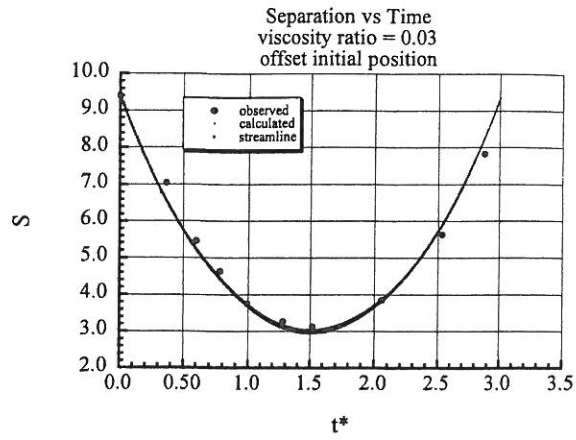

(a)

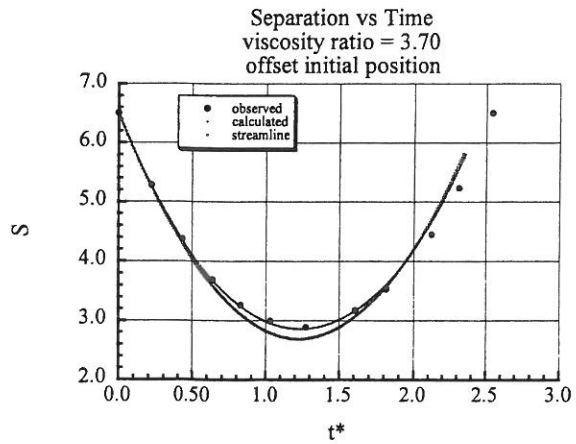

(b)

FIG. 7. Time dependence of S for drops offset from the inflow axis (a) $\lambda = 0.03$, (b) $\lambda = 3.70$.

this. As the viscosity ratio is increased to 3.70, however, the hydrodynamic interaction increases. The increased interaction then shifts the minimum separation to a larger distance than is predicted for two hypothetical drops that follow the undisturbed streamlines. Even though the experimental drops are slightly deformed due to the undisturbed velocity gradient (Taylor deformation, $D_f = 0.043$), the theoretical calculations for spherical drops capture the increased interaction and accurately maps the "shape" of the relative trajectory and the time dependence of ϕ and s. It is important to note for drops without close contact ($s > 2$) that the relative trajectories are symmetric about $\phi = 90°$. It will be shown in Sec. IV C that when drops come into close contact ($s = 2$ or less) this symmetry is broken due to the additional interfacial deformation that occurs as a consequence of the "collision" process.

C. Colliding drops

In this section, we probe the effects of close contact and flow-induced deformation on the trajectories of two drops. We define close contact or "collision" when the separation between the drops is no longer visible. The capillary number varies between 0.0064 and 0.0968, which produces flow-induced deformations of the drops, prior to any significant interaction, between $D_f = 0.02$ and 0.22. Guido and Simeone[8] observed a significant variation in the deformation parameter during the collision of two drops in shear flow. In this work, the deformation remained constant throughout the interaction.

Figures 9 and 10 show the "shapes" of the relative trajectories (s vs ϕ) for drops with a viscosity ratio of 0.03 at four capillary numbers. The initial orientations of the drops are aligned with the inflow axis and close-contact occurs. From Figs. 9 and 10 we observe that the minimum distance between drop centers (nondimensionalized with the undeformed drop radius) is less than two and decreases with increasing capillary number. This is a result of the flow-induced deformation. Within error, the measured separation distance corresponds to the minor axis of the deformed drops. Since no coalescence is observed, there presumably remains a thin film between the drops in all cases. The insert

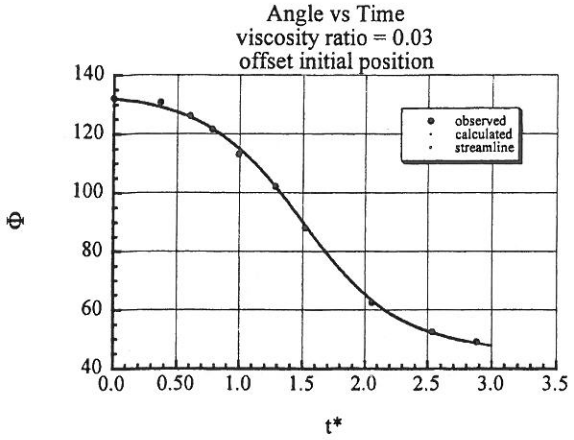

(a)

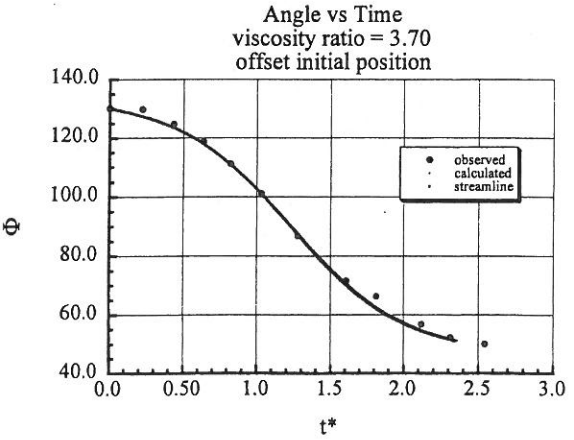

(b)

FIG. 8. Time dependence of ϕ for drops offset from the inflow axis (a) $\lambda = 0.03$, (b) $\lambda = 3.70$.

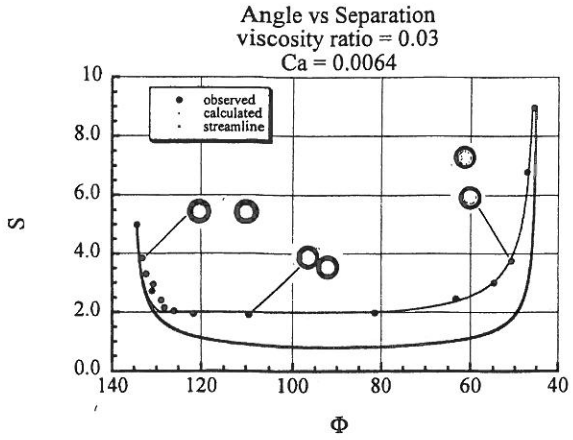

(a)

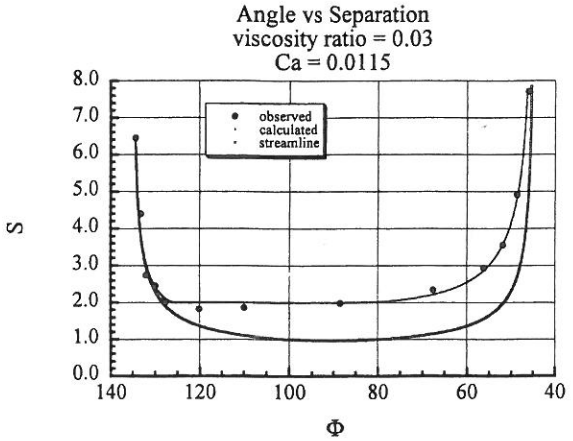

(b)

FIG. 9. Relative trajectories, S vs ϕ, for different capillary numbers with $\lambda = 0.03$. (a) Ca$=0.0064$, $D_f = 0.02$; (b) Ca$=0.0115$, $D_f = 0.036$.

in Fig. 10 for a capillary number of 0.0579 shows a case where s is less than two and a visible separation between the drops exists. From Figs. 9 and 10 we observe that the experimental trajectory curves are asymmetric, with the minimum separation occurring at an orientation angle (ϕ) which is greater than 90°. The asymmetry of these trajectories arises from the additional interfacial deformation that develops when the drops are in close contact. As the drops are pushed together, the interfaces of the drops flatten, which increases the interfacial area between the two drops, reduces the rate of film drainage, and forces the drops to remain separated. Clearly, the increased time for film drainage is sufficiently longer than the "collision" time at close contact that coalescence is not observed. In addition to inhibiting coalescence, the interfacial deformation produces an irreversible interaction between the two drops. If, after close contact, the flow is reversed, the trajectories are shifted to larger minimum separations. This is evident from Figs. 9 and 10 where the observed exiting trajectories are significantly shifted from the streamline corresponding to the initial position of the drops (i.e., at equivalent angles, such as 130° and 50°, the separation along the exit trajectory is larger than the separation along the approach trajectory). This shift is such that the minimum separation would be increased if the flow were reversed. This irreversible interaction is only observed experimentally for trajectories with close contact. For trajectories without close contact, such as in Fig. 6, any asymmetry of the trajectories is too small to be measured within the accuracy of the present experiments. This is due to the fact that the interaction process produces only infinitesimal deformation beyond the constant degree of deformation that is caused by the undisturbed velocity gradient.

The calculated trajectories in Figs. 9 and 10 indicate that the low viscosity ratio spherical drops essentially approach following streamlines and collide (when $s=2$) after only a slight rotation. At this point, the *ad hoc* modification discussed previously is implemented and the drops rotate with $s=2$ until $\phi<90°$. When $\phi=90°$ the complete spherical theory is resumed and the exiting trajectory for spheres is predicted. Overall, the spherical theory, including this *ad hoc* modification, predicts the shape of the relative trajectories quite well. For Ca$=0.0064$ where the deformation of the

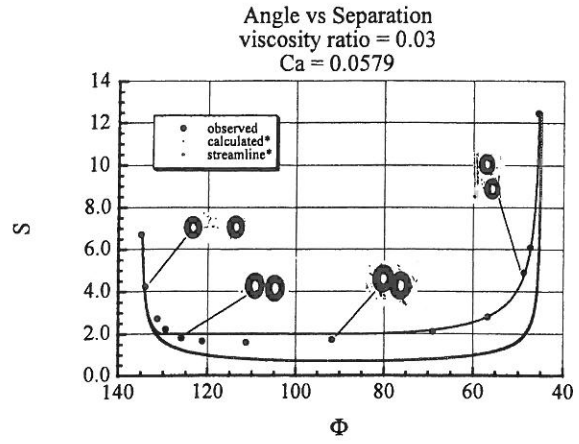

(a)

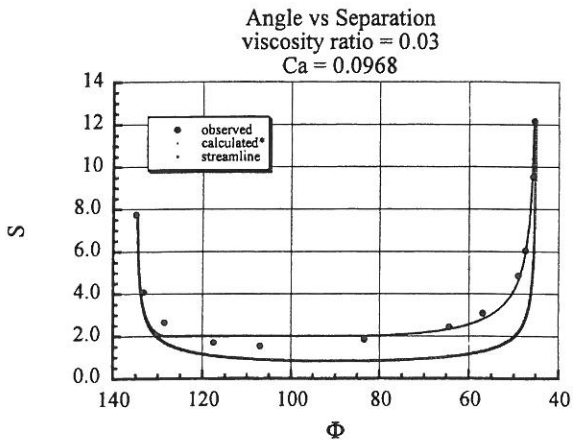

(b)

FIG. 10. Relative trajectories, S vs ϕ, for different capillary numbers with $\lambda=0.03$. (a) Ca$=0.0579$, $D_f=0.136$; (b) Ca$=0.0968$, $D_f=0.22$.

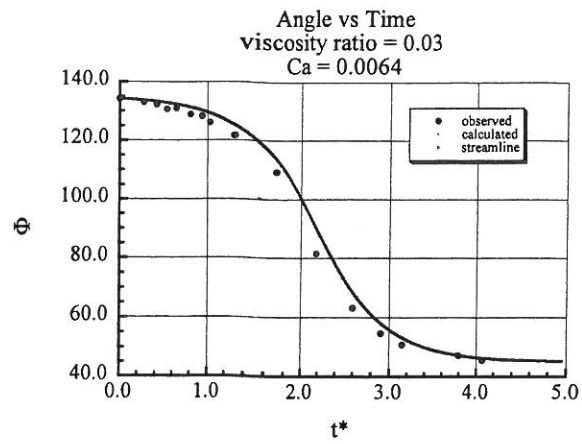

(a)

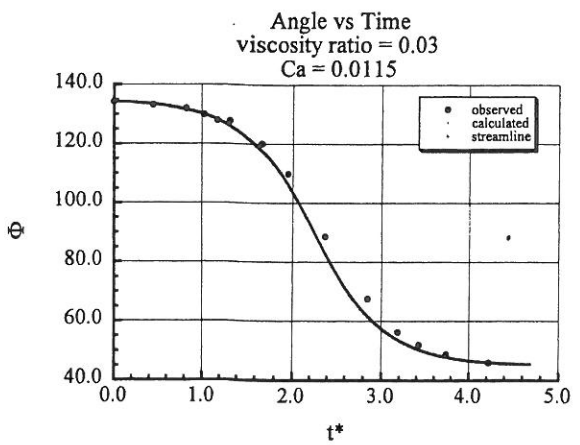

(b)

FIG. 11. Time dependence of ϕ for different capillary numbers with $\lambda=0.03$. (a) Ca$=0.0064$, $D_f=0.02$, (b) Ca$=0.0115$, $D_f=0.036$.

drops is minimal ($D_f=0.02$) and the drops are nearly spherical, the experimental results and the spherical theory are in excellent agreement. At higher capillary numbers similar agreement between the experimental results and the spherical theory is observed even though the flow-induced deformation has increased. The theoretical calculations do deviate from the experimental results near the minimum separation, because when the *ad hoc* modification to the calculated trajectories is implemented, the "calculated" separation remains at two while the experimental separations drop below two due to flow-induced deformation. However, in spite of the difference in s at $\phi=90°$ (i.e., $s=2$ in the theory, but $s<2$ experimentally), the shape of the exiting trajectories (s vs ϕ for $\phi<90°$) shows excellent agreement with the experiments. This is quite interesting. It indicates that the exiting trajectories for two drops in planar extensional flow are defined by the theoretical trajectory for spherical drops with initial values, $s=2$ and $\phi=90°$, regardless of the drop deformation induced by the undisturbed velocity gradient. For the relative trajectories shown in Figs. 9 and 10, the modified spherical theory reproduces the approaching and exiting trajectories of deformed drops with deformations up to 0.22 and capillary numbers up to 0.0968.

Of course, the results and theoretical comparisons shown so far in Figs. 9 and 10 relate only to the shapes of the relative trajectories. A more critical and potentially useful test is the time dependence of ϕ and s for the experimental results shown in Figs. 9 and 10. Results for ϕ and s vs time are shown in Figs. 11–14. For the viscosity ratio of 0.03 considered in Figs. 11–14, the relative mobility function perpendicular to the line of center, $B(s)$, remains small and the drops rotate as if there is little or no interaction as shown by the overlap of the calculated and streamline curves. The calculated time dependence of ϕ agrees with the experimentally observed dependence, which indicates that the deformation does not affect the rotation rates of the drops. As the viscosity ratio increases, the value of $B(s)$ increases to non-negligible values, and the hydrodynamic interaction retards the rotation rate of the two drops. Figure 15 shows the time dependence of ϕ and s for a viscosity ratio of 3.70. The calculated and observed dependence is in good agreement. Both show that two hydrodynamically interacting drops ro-

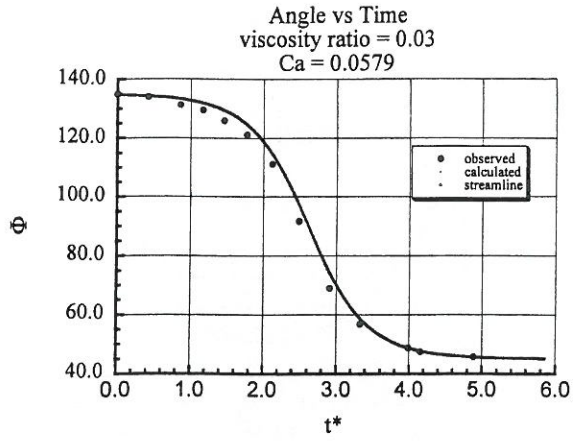

(a)

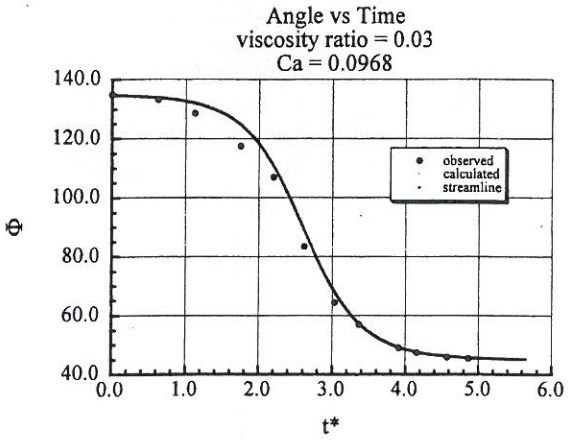

(b)

FIG. 12. Time dependence of ϕ for different capillary numbers with $\lambda = 0.03$. (a) Ca=0.0579, D_f=0.136; (b) Ca=0.0968, D_f=0.22.

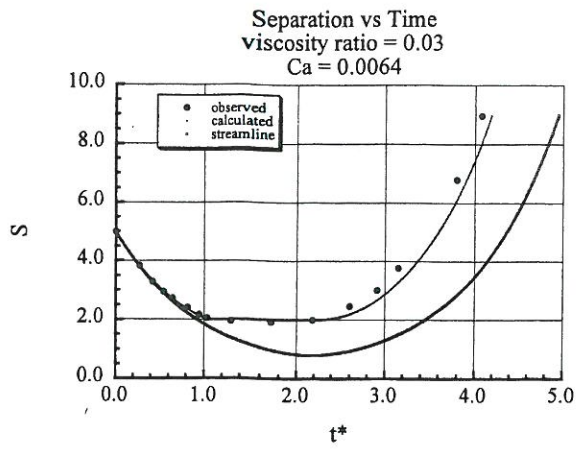

(a)

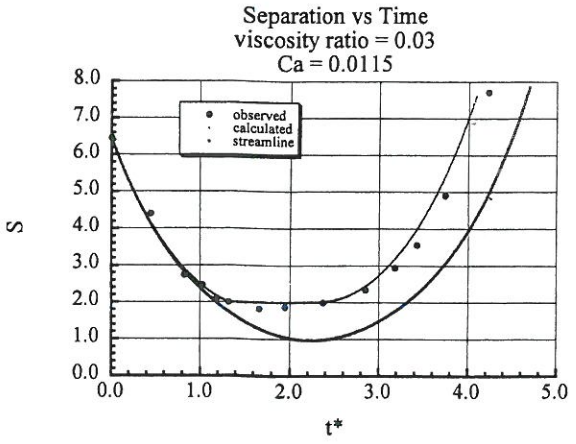

(b)

FIG. 13. Time dependence of S for different capillary numbers with $\lambda = 0.03$. (a) Ca=0.0064, D_f=0.02; (b) Ca=0.0115, D_f=0.036.

tate slower than two hypothetical drops that affinely follow streamlines of the undisturbed flow. While $B(s)$ remains small during the interaction of 0.03 viscosity ratio drops, the relative mobility function along the drops' line of center, $A(s)$, increases as the separation is reduced. In addition, the *ad hoc* modification to the calculated solution forces $s=2$ until sufficient time has elapsed for the drops to rotate to an angle which is less than 90°. Therefore, we expect the calculated and the observed time dependence of s to deviate from the time dependence of two hypothetical drops that affinely follow streamlines of the undisturbed flow for all values of λ, and this is observed in Figs. 13–15. Even though the calculated and observed separations differ during close contact for the reasons explained previously, the "*ad hoc*" modification to the theory for spherical drops accurately captures the time dependence of the approaching and exiting drop trajectories and accurately predicts the total period that the drops are in close contact. This predicted interaction time can be incorporated into studies which estimate coalescence probabilities.

V. DISCUSSION

A. Asymmetry of the trajectory curves

As stated earlier, when the two drops are in close contact, the asymmetry in the experimental trajectories arises from the additional interfacial deformation that develops between the two drops. We now give a brief explanation for this. When the drops are in the compressional quadrant of the flow, the external flow field pushes the drops together and the additional interfacial deformation develops from the pressure that is required to force the fluid from the gap between the two drops. As the drops rotate into the extensional quadrant, the flow field no longer pushes the drops together, but acts to separate the drops. While the effects of the external flow field have reversed, the additional interfacial deformation that developed in the compressional quadrant still exists. With this additional deformation the drop shape is unsteady and the interfacial tension drives the drop back to its steady-flow induced shape. This motion acts to push the drops away from each other. Thus, in the compressional quadrant the development of the additional interfacial defor-

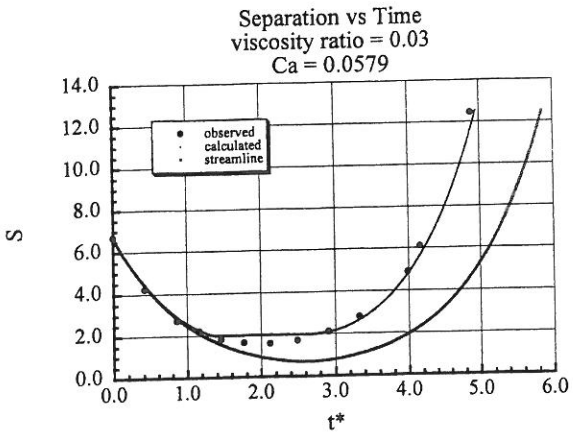

(a)

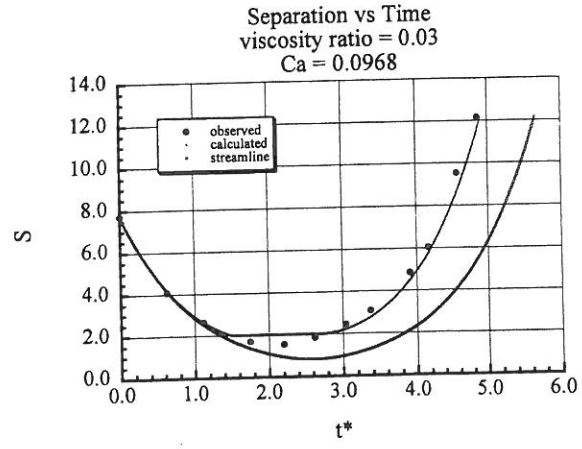

(b)

FIG. 14. Time dependence of S for different capillary numbers with $\lambda = 0.03$. (a) Ca$=0.0579$, $D_f=0.136$; (b) Ca$=0.0968$, $D_f=0.22$.

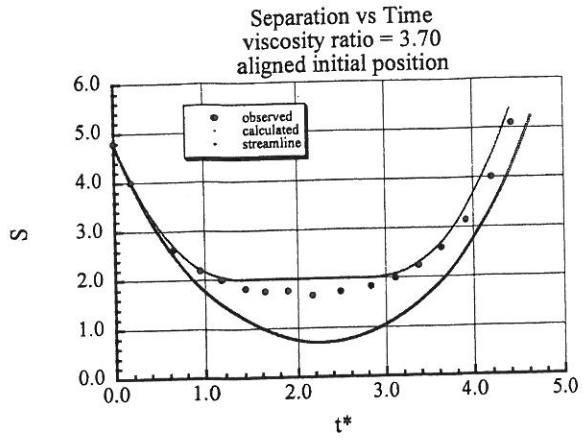

(a)

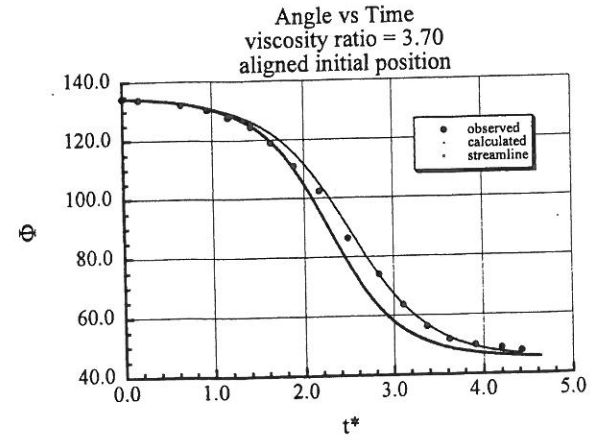

(b)

FIG. 15. Time dependence of S and ϕ for $\lambda = 3.70$ drops in close contact.

mation retards the approach of the two drops, while in the extensional quadrant, the additional interfacial deformation accelerates the separation of the two drops. This results in the asymmetry in the separation as a function of time and angle.

B. The *ad hoc* modification

Experimentally, we show that the modified theory for spherical drops accurately predicts the relative trajectories and the time dependence of s and ϕ for planar extensional flow. This is consistent with the numerical work of Lowenberg and Hinch,[3] who showed for shear flow that the modified theory for spherical drops is accurate for small capillary numbers and modest deformations. Without the *ad hoc* modification, we would be unable to calculate the complete time dependence of s and ϕ with the theory for spherical drops. It is intriguing that the *ad hoc* modification provides a reasonable estimate of the interaction time and accurately maps the rotation of the two drops in the flow field. The fact that ϕ is mapped accurately in time with the *ad hoc* modification implies that the rotation of two touching deformed drops is equivalent to the rotation of two touching spherical drops. It is not obvious that this should be true. A possible explanation may be that the deformed drops have a smaller center to center separation and a narrower profile than two spherical drops and that the smaller separation and narrower profile compensate for each other equally.

C. Coalescence

As stated previously, coalescence was not observed for the range of capillary numbers and viscosity ratios examined in this study. The absence of coalescence, however, does not imply that we are in a capillary regime where coalescence does not occur. As the drops are pushed together, the drop interfaces deform and a thin film develops between the drops. This thin film must drain to a critical thickness for the film to collapse. This critical thickness is the length scale of attractive nonhydrodynamic interdroplet forces and is independent of the drop radius. Thus, for coalescence to occur the interaction time must exceed the time for film drainage down to the critical thickness.

For a given initial position and flow type, the purely hydrodynamic interaction and collision process is identical

for drops of any size provided the capillary number and viscosity ratio are fixed. Thus, for a given viscosity ratio and capillary number the drops' shape, the interaction time, the geometry of the thin film between the two drops, and the minimum film thickness are identical on a dimensionless basis. Since the critical film thickness is independent of the drop radii, the question is, for what size drops (if any) does the dimensionless minimum film thickness correspond to a physical length scale that is less than the critical value for coalescence? For the capillary numbers and relatively large drop sizes examined in this work (radii of approximately 1 mm), the dimensionless minimum film thickness corresponds to a dimensional distance that is larger than the critical film thickness. A substantially smaller drop at similar capillary numbers with an identical nondimensional minimum gap as in these experiments can have an actual dimensional film thickness on the same order as the critical film thickness and thus coalesce. With this in mind, there should be a size dependence on the critical capillary number for coalescence with the critical capillary number decreasing with increasing drop size.[12] Preliminary studies of micron size drops in planar extensional flow at similar (or larger) capillary numbers as in this work have shown coalescence and indicate that the size dependence on the critical capillary number for coalescence does exists.

VI. CONCLUSIONS

This paper presents the results of an experimental study, which examines the trajectories of two purely hydrodynamically interacting drops or rigid spheres subjected to a planar extensional flow. By comparing the experimental results with the theory for spherical drops modified as described above, a number of conclusions can be drawn. First, the spherical theory accurately predicts the approach and exit trajectories of two drops even for drops with a substantial degree of flow-induced deformation. As a result, the spherical theory should provide an adequate estimate of the collision efficiencies for both spherical and moderately deformed drops. Second, for drops which do not come into close contact (the drops interact but remain sufficiently separated that no thin film forms), the spherical theory accurately predicts the symmetric trajectories and captures the increased hydrodynamic interactions for higher viscosity ratios, regardless of the flow-induced deformation. Third, for spherical or deformed drops, the spherical theory with the *ad hoc* modification provides a reasonable estimate of the maximum interaction time of two drops in close contact (i.e., the regime in which there is a thin film present). Fourth, for drops in close contact, the trajectory curves are asymmetric and irreversible with a minimum separation which corresponds approximately to the minor axis of the deformed drops and is less than the minimum separation of two spheres ($s=2$).

Thus, the existing trajectory theory for spherical drops provides a reasonable estimate of the trajectories and interaction time of two deformable drops with or without close contact, provided we include the "*ad hoc*" extension to this theory that is described herein.

ACKNOWLEDGMENTS

Special thanks to Alexander Zinchenko and Robert Davis for providing the FORTRAN code, which calculates the relative mobility functions, $A(s)$ and $B(s)$, for spherical drops. This work has been supported by a grant from the Microgravity Program of NASA.

[1] G. K. Batchelor and J. T. Green, "The hydrodynamic interaction of two small freely-moving spheres in a linear flow field," J. Fluid Mech. **56**, 375 (1972).
[2] H. Wang, A. Z. Zinchenko, and R. H. Davis, "The collision rate of small drops in linear flow fields," J. Fluid Mech. **265**, 161 (1994).
[3] M. Lowenberg and E. J. Hinch, "Collision of two deformable drops in shear flow," J. Fluid Mech. **338**, 299 (1997).
[4] A. Z. Zinchenko, M. A. Rother, and R. H. Davis, "A novel boundary-integral algorithm for viscous interaction of deformable drops," Phys. Fluids **9**, 1493 (1997).
[5] M. Manga and H. A. Stone, "Collective hydrodynamics of deformable drops and bubbles in dilute low Reynolds number suspensions," J. Fluid Mech. **300**, 231 (1995).
[6] X. Zhang, R. H. Davis, and M. F. Ruth, "Experimental study of two interacting drops in an immiscible fluid," J. Fluid Mech. **249**, 227 (1993).
[7] M. Manga and H. A. Stone, "Buoyancy-driven interactions between deformable drops at low Reynolds numbers," J. Fluid Mech. **256**, 647 (1993).
[8] S. Guido and M. Simeone, "Binary collision of drops in simple shear flow by computer-assisted video microscopy," J. Fluid Mech. **357**, 1 (1998).
[9] B. J. Bentley and L. G. Leal, "An experimental investigation of drop deformation and breakup in steady, two-dimensional linear flows," J. Fluid Mech. **167**, 241 (1986).
[10] W. J. Milliken and L. G. Leal, "Deformation and breakup of viscoelastic drops in planar extensional flows," J. Non-Newtonian Fluid Mech. **40**, 355 (1991).
[11] H. A. Stone and L. G. Leal, "Relaxation and breakup of an initially extended drop in an otherwise quiescent fluid," J. Fluid Mech. **198**, 399 (1989).
[12] A. K. Chesters, "The modelling of coalescence processes in fluid liquid dispersions—a review of current understanding," Chemical Engineering Res. and Design, **69**, 259 (1991).